Available online at www.sciencedirect.com
SCIENCE DIRECT®
Journal of Molecular Catalysis A: Chemical 216 (2004) 83–99
JOURNAL OF MOLECULAR CATALYSIS A: CHEMICAL
www.elsevier.com/locate/molcata

Steam promoted mesoporosity in USY zeolites: structural properties and 1,2,4-TMB reactivity

G. Tonetto [a], M.L. Ferreira [b,*], H. de Lasa [a]

[a] *Faculty of Engineering Science, Chemical Reactor Engineering Center, University of Western Ontario, London, Ont., Canada N6A 5B9*
[b] *Chemical Engineering Department, PLAPIQUI, UNS-CONICET, Camino La Carrindanga km 7, CC 717, 8000 Bahía Blanca, Argentina*

Received 14 November 2003; received in revised form 4 February 2004; accepted 6 February 2004

Available online 15 April 2004

Abstract

This work addresses the potential effects of steaming in the case of dealumination of Y zeolites. With this end, the interaction between 1,2,4-trimethylbenzene (1,2,4-TMB) and ultrastable Y zeolite (USY) is analyzed. The zeolite is modeled using the complete exposed USY structure of one unit cell constituted by eight sodalite cages, 16 hexagonal prisms bridging the sodalite cages and the formed supercage.

The MM2 method is considered to evaluate the steric energies in a model of the window including the six surrounding complete sodalite cages. The Parametrized Model revision 3 (PM3) method is also used to analyze the changes in enthalpy upon 1,2,4-TMB adsorption and reaction on each cage. Finally, several calculations on the adsorption of the 1,2,4-TMB on different sodalite cages are effected using the Extended Hückel method and this to complete the description about the interactions between the crystalline USY and 1,2,4-TMB molecules.

Calculation results reported in this work support the high probability of carbocation formation and overall reaction in fragments removed from the zeolite. This partially destroyed zeolite display some relaxation of the original structure and allows extra accessibility of TMB to the acidic sites.

Keywords: USY; Trimethylbenzene; Hydrocarbon cracking; MM2; PM3; EHMO

1. Introduction

Zeolites catalyze a wide variety of chemical reactions. In the petrochemical industry, ultrastable Y zeolites (USY) are largely used for processes such as cracking, isomerization and alkylation of hydrocarbons. Despite the considerable advancements in the FCC technology and the studies developed in catalysts and reaction mechanisms, still more research is needed, and this to clarify the exact type of active sites and the nature of reaction pathways.

Y-zeolites are synthesized with low Si/Al ratio between 2.5 and 2.9. After hydrothermal treatment, global and framework Si/Al ratios are 2.8 and 11, respectively [4].

Beyerlein et al. [1] summarize the formation of USY as a two-step process: (a) first, there is an expulsion of Al atoms from framework T-sites, (b) second, these formed vacancies via Al expulsion are, to a great extent, refilled by Si atoms migrating from the collapsed portions of the crystals. If this "healing" did not occur, the entire zeolite crystal could collapse. In addition, parts of the structure that provide the silicon for this substitution, may be destroyed, forming mesopores partially filled with amorphous debris [2].

From three-dimensional transmission electron microscopy (3D-TEM) studies, Janssen et al. [35] observed that the mesoporous system is primarily formed through cavities inside the crystals and not through pores connecting the interior of the crystals with the external surface. This is a consequence of mobile silicon species from defect sites (where aluminum has been extracted) which cause some defect sites to develop into cavities in the zeolite crystals and other defect sites to vanish by healing the framework. Thus, Lewis acid sites are formed ejecting Al from the framework. The nature of this extraframework Al (EFAL), formed during steaming, has been the subject of research and several candidate chemical species forms have been proposed with aluminum present as cations Al^{3+}, AlO^{+}, $(Al)(OH)_2{}^{+}$ $Al(OH)^{2+}$ or neutral or polymerized forms AlOOH, $Al(OH)_3$ and Al_2O_3 (review in [3]).

Gola et al. [4] quantified the EFAL species using NMR and XRD. USY steamed at 923 K contains 34 EFAL per unit

* Corresponding author. Tel.: +54-291-4861700; fax: +54-291-4861600.
E-mail address: mlferreira@plapiqui.edu.ar (M.L. Ferreira).

1381-1169/$ – see front matter © 2004 Elsevier B.V. All rights reserved.
doi:10.1016/j.molcata.2004.02.010

cell. Among these, around six are linked to the framework in distorted tetrahedral geometry. Approximately 12 EFAL per unit cell are in the form of isolated aluminum containing ions. The remaining 17 EFAL, which include Al^{V} and Al^{VI}, are present as amorphous material. Thus, the polymeric amorphous material, responsible in the steamed sample for pore blocking and loss of crystallinity, contains at most one half of the EFAL.

Concerning the Al species in zeolites, Fripiat and coworkers [5] found two types of Lewis acid sites using HRAlNMR and CO FTIR: a tetrahedral and a pentagonal site. In addition, some unspecified synergism between Brönsted acid sites with Lewis acid sites was reported with this synergism associated with Al, described as a super acidity [6].

Results of a study of the effect of trivalent cation exchange in clean frameworks provide evidence that EFAl are highly dispersed and exist as cationic species in the small cages [7] with these species not being reflected in the direct measurement of solid acidity. Furthermore, calorimetric studies have failed to find evidence for super acidic Brönsted sites [8].

Regarding the effect of steam dealumination of a zeolite on its hydrocarbon cracking activity, Keuhne et al. [36] reported that the 2-methylpentane cracking turnover frequencies (TOFs) for chemically dealuminated USY was five times larger than HY, while the TOF of USY, dealuminated by steam, was 80 times higher, with the differential heat of ammonia adsorption on these zeolites being nearly constant. These results strongly suggest that cracking activity may be affected by other causes in addition to acid strength.

These authors [9–11] also indicated that although new hydroxyl-groups are formed, which are physically different from the original hydroxyls associated with the aluminums of the framework, there is no evidence that these new groups have an effect in the catalyst properties. In particular, when compared under the same conditions (alkane conversion, temperature, and partial pressures), the product distributions in the cracking reaction are very close and unaffected by steaming. Furthermore, it was also observed for the monomolecular cracking that the intrinsic activation energy for the formation of the carbonium ion-like transition state, as well as the turnover rates remains, on this basis, unaffected by steaming [10]. Moreover, it is postulated that the large effect of steaming on the apparent catalytic activity is mainly due to the formation of mesopores, cracks and other structural defects that increase the external (accessible) surface area of the zeolite crystallite, and correspondingly reduce the influence of the pore diffusion-limited cracking reactions.

Associated with this, there are well-documented reports about the partial destruction of the zeolite framework with formation of mesopores [12,13]. In this respect, the formation and evolution of mesopores were recently studied by combination of high-resolution electron microscopy (HREM) and analytical electron microscopy (AEM) with high-resolution ^{27}Al NMR (HRNMR) [34]. It was revealed in this manner that the extracrystalline phase represented by dark bands, is the main contributor to the EFAL species, tetrahedral, pentacoordinate and octahedral.

Concerning isomerization and catalytic cracking, three mechanisms can be postulated [11]: monomolecular, bimolecular, and oligomeric bimolecular cracking. The monomolecular mechanism [14] involves a Brönsted acid site with the protonation of an alkane leading to the formation of a pentacoordinated carbenium ion (carbonium). Regarding aromatic molecules, protonation of the aromatic ring is a relatively easy step, leading to tetrahedral carbon and to a delocalized positive charge in another carbon (formation of carbenium ion). Carbons carrying substituent, stabilizing this charge (alkyl groups), are the preferred location for the positive charge. The shift of alkyl groups from carbon to carbon concerted with an H shift, produces the isomerization with this process being completed with the Brönsted acid site regenerated via proton transfer.

The classical bimolecular mechanism [15] involves a carbenium formation on a Brönsted acid site. When this mechanism takes place with alkyl-substituted aromatics, the end result is a disproportionation product with lower or higher alkyl groups in the aromatic ring. The classical ‘transfer step’ can involve a H or an alkyl group transfer from another molecule. So, the bimolecular mechanism includes an exchange H*H or H*alkyl, with the carbenium which can eventually be subjected to further isomerization. The process is completed here with proton transfer regenerating the Brönsted active site or being directed to another neutral alkyl–aromatic molecule.

The oligomeric cracking mechanism [11] includes a step of oligomerization via carbenium ions, which are formed by alkylation of a smaller carbenium ion with the overall rate being a function of external (accessible) zeolite surface area. Higher conversions enhance the alkylation reaction and oligomerization at the surface increasing the number of sites for H transfer with the reactant. Coke deposition is then promoted as a result of the alkylation step becomes faster that the scission step. So, the size of the surface oligomeric species continues to grow and lead to highly condensed aromatic molecules, the precursors of coke.

This work examines the first step of 1,2,4-trimethylbenzene (1,2,4-TMB) and USY zeolite interaction, using MM2, Parametrized Model revision 3 (PM3) and EHMO methods. It is considered that 1,2,4-TMB adsorbs on acidic active sites with subsequent carbocation formation. Al atoms are examined at two principal locations: (a) outside the crystalline structure (USY structure with a 7.4 Å window diameter), (b) at the mesopores, which are formed during steam dealumination [1,16]. Models of the USY-cages are considered to represent these two situations.

2. General approach

Concerning zeolite structures, modeling can only be developed for the so-called “clean surfaces” of the USY

framework, free of amorphous phase constituents. These "clean surfaces" of USY zeolites can provide valuable steric and electronic information.

With this end, a complete exposed structure of one unit cell constituted by eight sodalite cages, 16 hexagonal prisms bridging the sodalite cages and the formed supercage were considered. The experimental Si/Al ratio was used and the EFAL distribution was the one reported by Grace in the crystalline portion of USY [17] and Gola et al. [4] in a USY sample steamed at 923 K.

The alkyl aromatic compound of specific interest is the 1,2,4-TMB. In this respect, it is useful to explore the first step of different isomerization possibilities of this molecule, using zeolite USY to produce the 1,2,3-TMB and 1,3,5-TMB isomers. The main idea here is to consider that Brönsted acidity is the responsible of the initial protonation and carbenium ion formation.

Thus, while the access of the 1,2,4-TMB to the supercage is studied, the isolated sodalite cages are analyzed in order to test the steric and repulsion energies and changes in adsorption enthalpies with different species intermediary formation (carbocations and covalent bond).

Also, an alkoxide bond is investigated between the zeolite surface and 1,2,4-TMB. This kind of alkoxide species was proposed by Kazansky and Senchenya [18]. Furthermore, in the case of USY zeolites, even the Lewis acid sites may intervene in the reaction through dehydrogenation on EFAL sites. This could be associated to the abstraction of hydride from one of the methyl groups of 1,2,4-TMB and the formation of a carbocation. This carbocation does not lead to monomolecular isomerization product but may provide an additional disproportionation route.

3. Theoretical methods

MM2 method was used to evaluate the steric energies in a model of the window including the six surrounding complete sodalite cages. The PM3 method included in the same package and MOPAC program was used to analyze the changes in enthalpy upon 1,2,4-TMB adsorption and reaction on each cage. Because of the qualitative nature of the Extended Hückel method, several calculations on the adsorption of the 1,2,4-TMB on different sodalite cages were included and this to complete the qualitative picture about the interactions between the crystalline USY and 1,2,4-TMB molecules.

3.1. PM3

PM3 is a reparametrization of Austin Model 1 (AM1). Hypervalent compounds are predicted with considerable improved accuracy and overall errors in formation enthalpies are reduced by about 40%. This method is a semiempirical procedure included in MOPAC with the following characteristics: (a) the basis set used in constructing the one-electron atom orbital is a minimum basis set of only the "s" and "p" Slater type orbitals (STOs) for valence electrons, (b) the core electrons are not explicitly treated. Instead, they are added to the nucleus and the nuclear charge is termed N effective, (c) many of the two-electron Coulomb and exchange integrals are parameterized based on the constitutive elements.

3.2. MM2

Chem 3D uses a modified version of Allinger MM2 force field. The principal addition to Allinger's MM2 force field is a charge–dipole interaction term, a quartic stretching term, Cutoffs for electrostatic and van der Waals terms with fifth-order polynomial switching function, automatic "pi" system calculations when necessary and torsional and non-bonded constraints. The parameter table of Chem 3 D contains many adjustable parameters that correct for the failing of many of the potential functions in outlying situations. Molecular mechanic energy is composed of the following terms.

3.2.1. Bond stretching energy

The stretching energy equation is based on Hooke's law. This energy is the contribution associated with the deformation of a bond from its equilibrium bond length. This energy calculation includes cubic and quartic stretch constants.

3.2.2. Angle bending energy

This energy is associated with deformation about an equilibrium bond angle.

3.2.3. Torsion energy

This term accounts for the tendency of dihedral angles to have and energy minimum occurring at specific intervals of $360/n$.

3.2.4. Non-bonded energy

Represents the pair wise sum of the energies of all possible interacting non-bonded atoms, i and j within a predetermined cut off distance. The non-bonded energy accounts for repulsive forces experienced between atoms at close distances and for the attractive forces felt at longer distances.

3.2.5. van der Waals energy

Repulsion is modeled by an equation, which combines an exponential repulsion with an attractive dispersion interaction ($1/R^6$), where R is obtained using the van der Waals radii of the atoms and an additional parameter that determines the depth of the attractive potential energy well and how easy is to push atoms together.

3.2.6. Electrostatic energy

When electrostatic energies are analyzed, there are three possible interactions accounted for by Chem 3D: charge/charge, dipole/dipole, charge/charge. Chem 3D does not use a distance dependent dielectric. As in the van der

Waals calculations Chem 3D invokes a fifth-order polynomial switching function in order to maintain second-order continuity in the force field.

3.3. EHMO

The molecular orbital calculations were carried out by means of an extended Hückel modified method (EHMO). This semiempirical procedure provides a useful preliminary approach. Thus, it has been used to study electronic changes and obtain qualitative trends in adsorption processes [19]. In this method, the non-diagonal elements of one electron extended Hückel–Hamiltonian are proportional to the overlap matrix elements.

The program used was ICONC, which was developed by Calzaferri and coworkers [20,21] and includes repulsive terms to the total energy, which are not explicitly included in the EHMO.

The repulsive Coulombic energy is taken into account in pairwise terms. The total energy (E_t) of our adsorbate/substrate system is expressed as

$$E_t = \sum n_i E_i + \frac{1}{2}\sum_i \sum_{i \neq j} E_{\mathrm{rep}(i,j)}$$

The first term in the preceding expression corresponds to the attractive valence electron contribution (n_i) and the second term to the pairwise interatomic repulsions. Each valence level i has an associated energy E_i with occupancy n_i. The repulsion energy of a nucleus i in the presence of a fixed atom j is calculated as an electrostatic term and the summation extended to all possible atom pairs (E_{rep}).

The experimental values for the ionization potentials involved in the calculations were obtained from published spectroscopic data [22] For the level 4p, there is only theoretical data in the literature, the data of Hartree–Fock–Slater was employed [23–25]. With respect to the atomic basic set, an s + p + d valence set of Slater type was employed. The values of the Slater exponents were obtained from Hoffmann [26] work. Atomic parameters used in EHMO calculations are listed in Table 1.

Table 1
Atomic parameters used in EHMO calculations

Atom	Orbital	Ionization potentials (eV)	Orbital exponents
Si	3s	−20.44	1.30
	3p	−12.41	1.60
O	2s	−31.60	2.163
	2p	−16.78	2.750
H	1s	−13.60	1.00
C	2s	−19.65	1.154
	2p	−11.13	1.451
Al	3s	−12.30	1.670
	3p	−6.50	1.383

The total energy of adsorbed species (or E_r) was calculated as the difference between the electronic energy of the system when the aromatic adsorbate is at a finite distance from USY model surface and when the molecule is far away from this surface, at an infinite distance with no interactions taking place.

The semiempirical molecular orbital calculations were performed in the framework of the cluster approximation that is the adsorption site and a portion of the otherwise infinite solid. The sectioning of the cluster from the rest of the lattice results in the appearance of the so-called dangling bonds and border effects. It was observed, in this respect, that while the electronic structure calculation converges rather slowly for the entire structure configuration, as the cluster size increases the chemisorption properties are satisfactory predicted [27].

3.4. The surfaces models

In this work, a complete exposed structure of one unit cell constituted by eight sodalite cages, 16 hexagonal prisms bridging the sodalite cages and the formed supercage were considered (Fig. 1). Thus, two kinds of models were considered: a complete model of the window, which includes six hexagonal cages (Fig. 1) and partial models of cages, considering especially the EFAL distribution (Figs. 3–6). Fig. 1 illustrate the *Complete Window* model, while Fig. 2 describes the *Reduced Window* model with *Cage 1*, *Cage 2*, *Cage 3*, and *Cage 4* referred here as partial models (Figs. 3–6).

All the six models include H, Al, Si and O atoms. From calculations of the minimization of the *Complete Window* model, Si–O bond length is close to 1.675 Å. For Al in the window, Al–O bond lengths are between 1.794 and 1.840 Å; and in case of Al–O–Si, the Al–O bond reaches 2.024 Å. In *Reduced Window* model, distances are estimated as follows: (a) Si–O between 1.629 and 1.635 Å, (b) Al–O (framework) at 1.822 Å, (c) Si–O–Al, at 1.66–1.664 Å for Si–O bond and at 2.006 Å for Al–O bond.

3.5. The molecule of 1,2,4-trimethylbenzene

The 1,2,4-TMB was modeled including all its atoms [28]. On this basis, the interactions of the 1,2,4-TMB to the external surface of the 7.4 Å-window were studied using the *Complete Window* model. 1,2,4-TMB configurations while approaching the 7.4 Å window are illustrated in schemes III and IV in Fig. 1B.

Furthermore, the *Cage* models allow the consideration of how the 1,2,4-TMB approaches collapsed regions of the zeolite structure. This can represent the mesoporous structures result of Si healing process result of the steaming [1].

Fig. 7 illustrates the 1,2,4-TMB approach to a cage with three possible molecular orientations: (a) with the aromatic ring parallel to the exposed surface (aromatic ring and surface orientated on the same *Y–X* plane), (b) with the aromatic

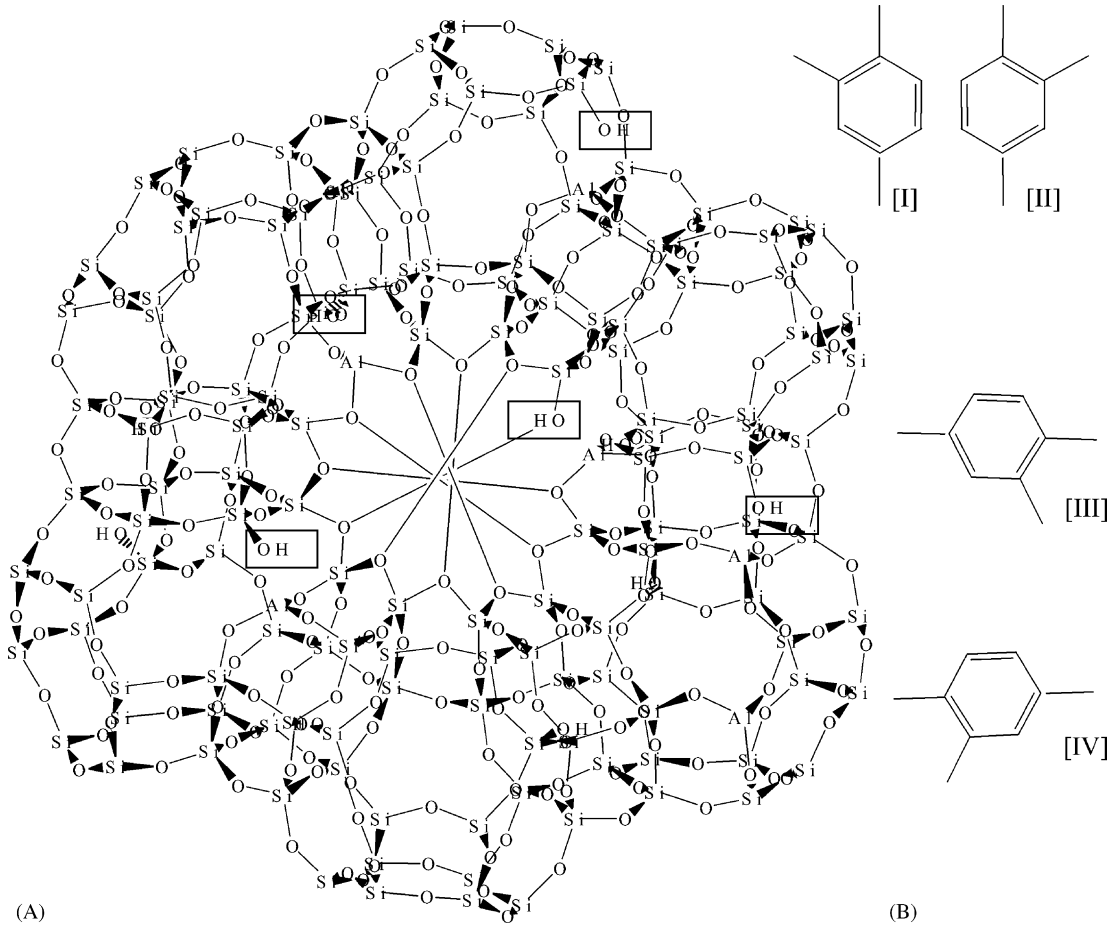

Fig. 1. (A) *Complete Window* model. The square box highlights the OH group under consideration. (B) 1,2,4-TMB configuration while approaching a *Complete Window* model: [I] 1H side, [II] 1H side, [III] and [IV] are the studied configuration in the 7.4 Å window.

ring perpendicular to the considered surface (aromatic ring in the *Y–X* plane to a surface in the *Y–Z* plane). This last case also accounts for two sub-cases: the 1,2,4-TMB approaches the surface via the one hydrogen side or two hydrogen sides of the aromatic ring (schemes I and II in Fig. 1B).

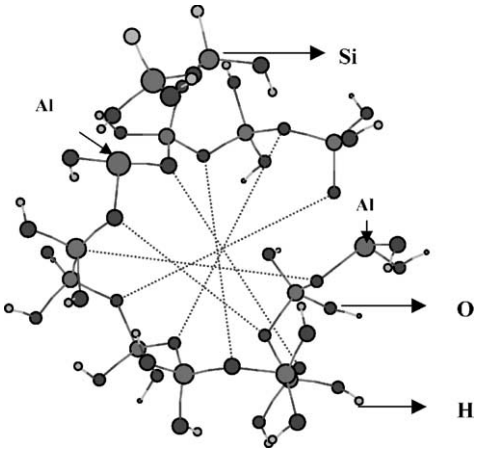

Fig. 2. *Reduced Window* model.

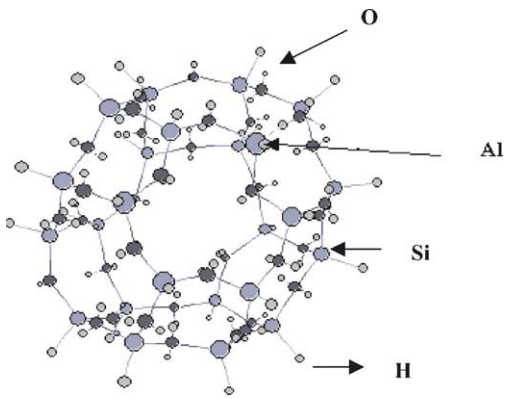

Fig. 3. *Cage 1* model.

4. The mechanism first step: the carbocation/alkoxide formation

Adsorption takes place on a Brönsted acid site with a carbocation being formed via H transfer. Two situations may occur: (a) carbocation ionic bond formation, (b) alkoxide covalent bond formation.

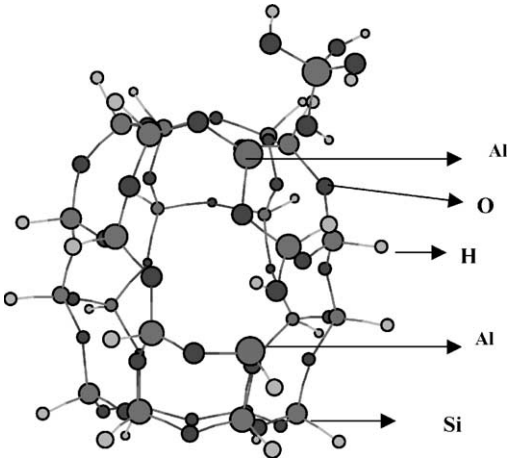

Fig. 4. *Cage 2* model.

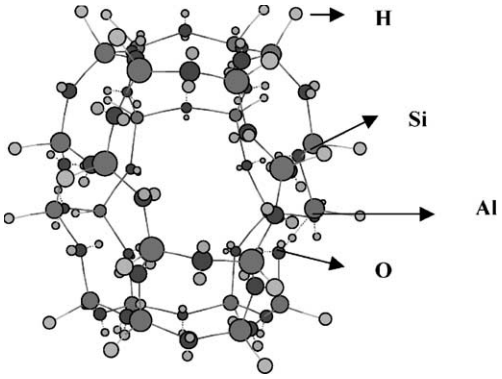

Fig. 5. *Cage 3* model.

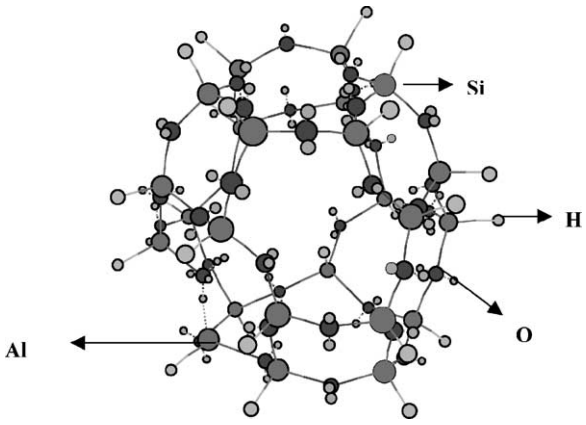

Fig. 6. *Cage 4* model.

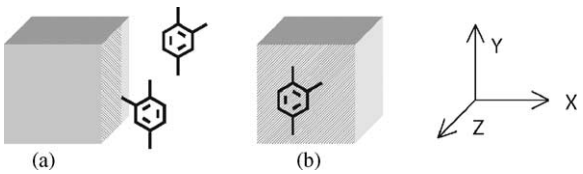

Fig. 7. TMB molecule approaching the surface: (a) aromatic ring parallel to the exposed surface, (b) aromatic ring perpendicular to the exposed surface. Exposed surface is highlighted as filled area with 45° diagonal.

Upon carbocation formation, the source Al–O–Si bond can potentially be disrupted. When this happens, the Al–O bond enlarges more than 3 Å. This implies that upon carbocation formation, changes in structure may take place leading to acidity losses and catalyst deactivation. This step included in the carbocation formation, allows obtaining enthalpy changes and steric energies with and without change in the Al–O bond.

4.1. The carbocation formation

The carbocation formation takes place by interaction of 1,2,4-TMB with a Brönsted acid site. These carbocations can undergo H/methyl shift and produce isomerization products by a monomolecular mechanism. Fig. 8 shows the structures of different carbocations that can be formed.

The so-called position 5 carbocation considers a TMB molecule approaching the USY surface by the 2H side. The overall result is a carbocation with the positive charge in position 6 (Scheme A, in Fig. 8).

The so-called position 3 carbocation involves a TMB molecule close to the surface by the 1H side. This leads to the addition of a proton in position 3 with a positive charge in position 6 (Scheme B, in Fig. 8).

Finally, position 6 also involves a TMB molecule approaching the USY surface by the 2H side, and leading to an H addition in position 6 with a positive charge in either positions 3 or 5 (Schemes D and C, respectively).

Both electronic and geometric effects influence the stabilization of the carbocation. For the approach to be effective a proper bond length between the OH group and the phenyl group has to be established allowing the H-transfer to occur. In this respect the 1,2,4-TMB approach by the 2H side, case of positions 5 and 6, is favored configuration. On the other hand, position 3 involves a TMB molecule approaching the site via 1H side with this carbocation not being favored by steric reasons.

In case of the attack of the proton in position 6, the location of the positive charge at the position 3 (case D) favors the methyl migration and exchange by H, producing 1,2,3-TMB. But this form implies a positive charge located far away from the surface, with an additional energy to produce the positive charge delocalization. Thus, it is expected that in this case the amount of 1,2,3-TMB isomer formed in TMB isomerization to be lower than the equilibrium composition.

Finally, the termination reaction requires a site receiving a proton or new 1,2,4-TMB molecule being protonated and generating a new carbocation.

In the case of the disproportionation reaction, a bimolecular interaction between carbocations can be considered as reported in Fig. 9. When the molecule is activated having a positive charge on a C atom, H or another methyl can interchange the methyl group associated to this C. Arrows indicate as H interchanges by methyl in the 1,2,3,5-TeMB formation with *p*-, *o*- and, *m*-xylenes formation (cases A–C,

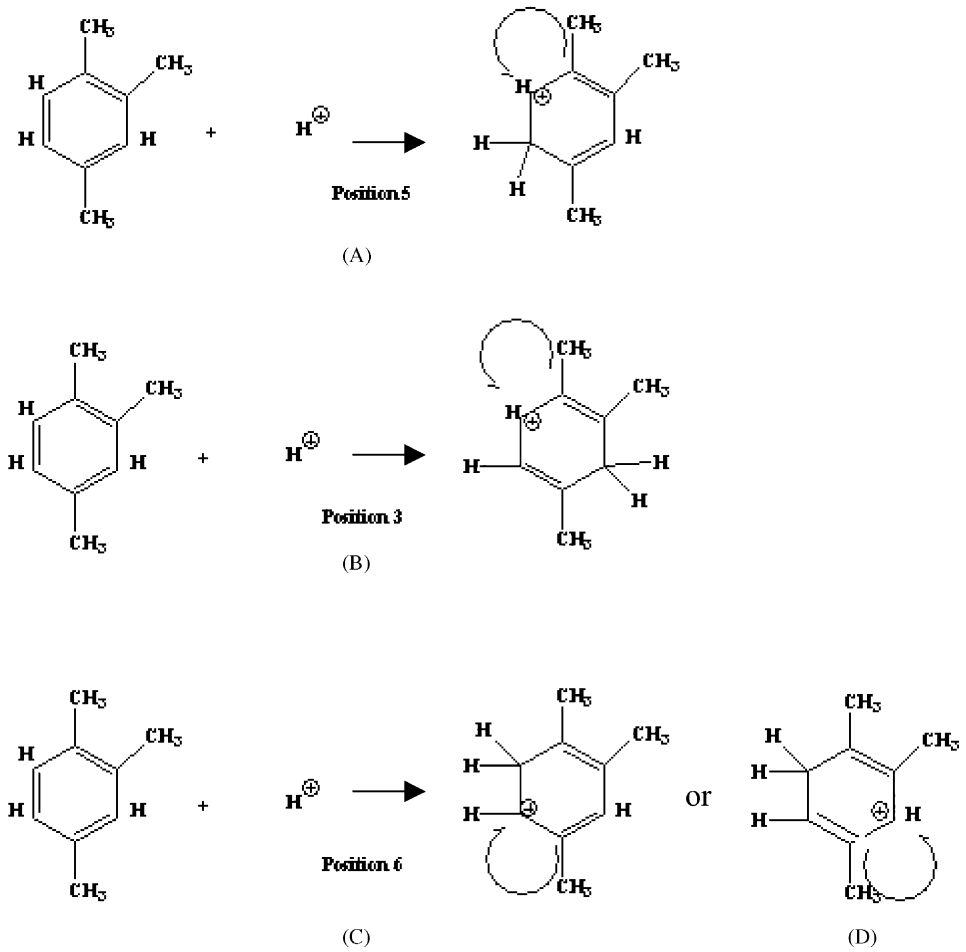

Fig. 8. Carbocation formation from TMB reaction with Brönsted acid sites: isomerization reaction.

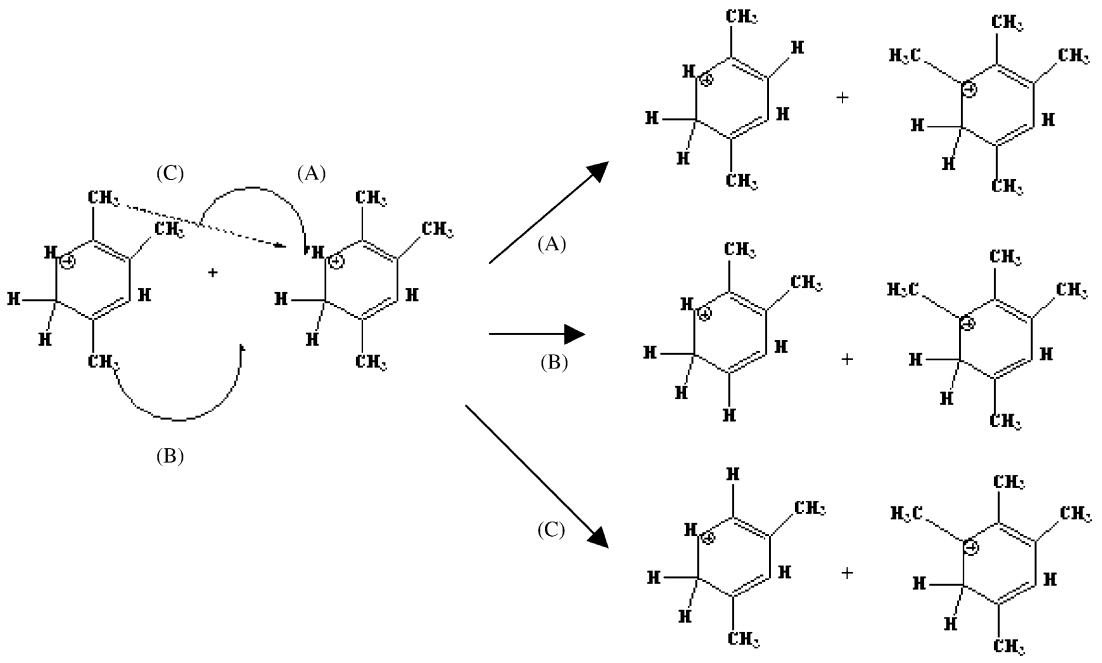

Fig. 9. Disproportionation reaction between two TMB carbocations.

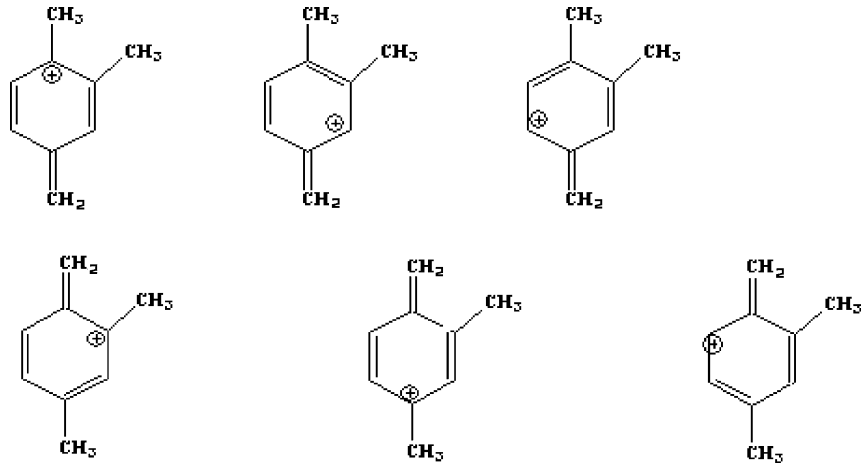

Fig. 10. Carbocations formed from 1,2,4-TMB by hydride abstraction by a Lewis acid site.

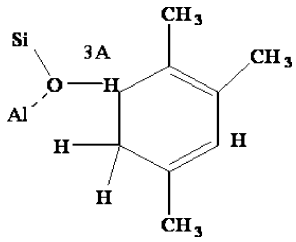

Fig. 11. Structure of a covalent alkoxide bond: C(TMB)–O(USY) bond.

respectively in Fig. 9). The termination step requires two sites receiving protons or new 1,2,4-TMB molecules being protonated, generating new carbocations.

On the other hand, when TMB molecule interacts with a Lewis acid site, a new kind of carbocations (schematized in Fig. 10) may be formed because of a hydride abstraction. These carbocations can further react with the carbocations generated via a Brönsted acid site and this may lead to a termination reaction step. No monomolecular isomerization is possible with this type of carbocation because the significant strength of the CH_2=phenyl group bond.

While the Lewis sites may favor disproportionation reaction, Brönsted acid sites are still required to generate the carbenium ions.

4.2. The alkoxide bond formation

An alkoxide bond can be considered between the zeolite surface and 1,2,4-TMB, as it was proposed by Kazansky and Senchenya [18] and described in Fig. 11. In order to test the importance of this possible alkoxide species, steric energy has to be evaluated and this involves the accounting of the carbocation reaction with Brönsted acid sites on the external structure of the USY zeolite.

5. Results

After establishing the most likely location of the 1,2,4-TMB adsorbed species, following the reaction between the intermediate carbocation and the OH of the a Si–OH–Al group, the following was considered:

(1) A carbocation–anion pair is formed on a USY structure with all bonds maintaining their original length.
(2) A carbocation–anion pair is produced with an altered USY structure with Al–O bond increased in length, and this as a result of the carbocation formation.
(3) An alkoxide C–O bond (close to 1.42 Å) is established with no USY structural changes and with all bonds keeping their original length.
(4) An alkoxide C–O bond (close to 1.42 Å) is formed on a modified USY structure with the Al–O bond increasing their length and this as a result of the alkoxide formation.
(5) A C–O enlarged alkoxide bond (∼3 Å) is established with an altered USY structure with the Al–O bond having an increased length and this as the consequence of the covalent alkoxide bond formation.

5.1. Modeling of the Complete Window

5.1.1. Modeling of the Complete Window—MM2

For the modeling of the *Complete Window*, the main approach was to calculate the changes in steric energies of the whole model and this when the molecule is introduced in the supercage and to assess also the reactions that can take place at the window (carbocation formation, alkoxide formation). Table 2 reports the resulting steric energies when the 1,2,4-TMB molecule is placed at the center of the 7.4 Å USY window, for the conformations referred as step 1 to 6 after energy minimization (Fig. 12).

Table 2
Steric energy for 1,2,4-TMB inside the supercage

	Step					
	1	2	3	4	5	6
Steric energy (kcal/mol)	1013.5	1024.4	1000.6	986.0	1032.4	1024.9

These steps 1 to 6 describe the different locations of the 1,2,4-TMB molecule as it moves from the outside of the supercage to the inside of the supercage. Moreover, as shown in Fig. 12, the preferred orientation for the 1,2,4-TMB molecule is the perpendicular orientation to the window plane with the parallel orientation for adsorption not likely to be favored.

Figs. 13 and 14 illustrate the different positions for carbocations formation outside the supercage as found via MM2 calculation. C1, C2 and C3 refer to the different locations of the carbocation within a fixed structural frame. C1–Al, C2–Al and C3–Al are used here to denote the models considering that the USY structure is relaxed upon carbocation formation. Table 3 also reports the steric energies and Al–OH (Si) bond length. It is apparent from Table 3 data that the steric energy is higher when the structure remains un-relaxed than when the relaxed configuration is allowed: 1130 kcal/mol (C2) versus 1075 kcal/mol (C1–Al).

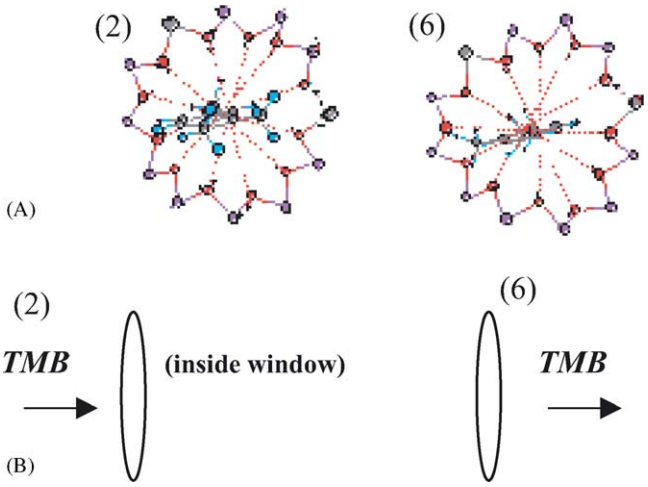

Fig. 12. Conformations 2 and 6 depicted: (A) front view, (B) schematic lateral view.

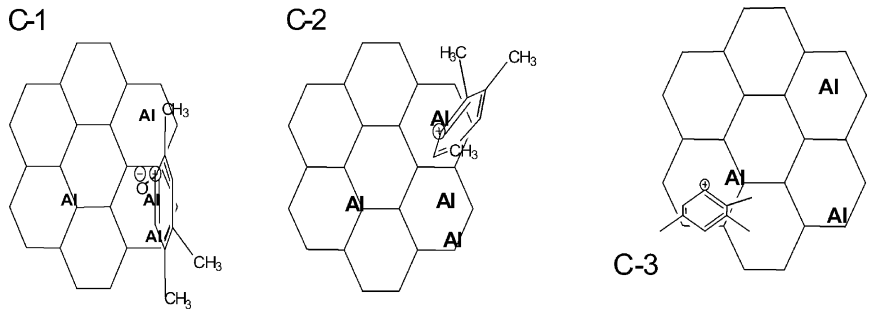

Fig. 13. Positions of carbocations formation outside the supercage.

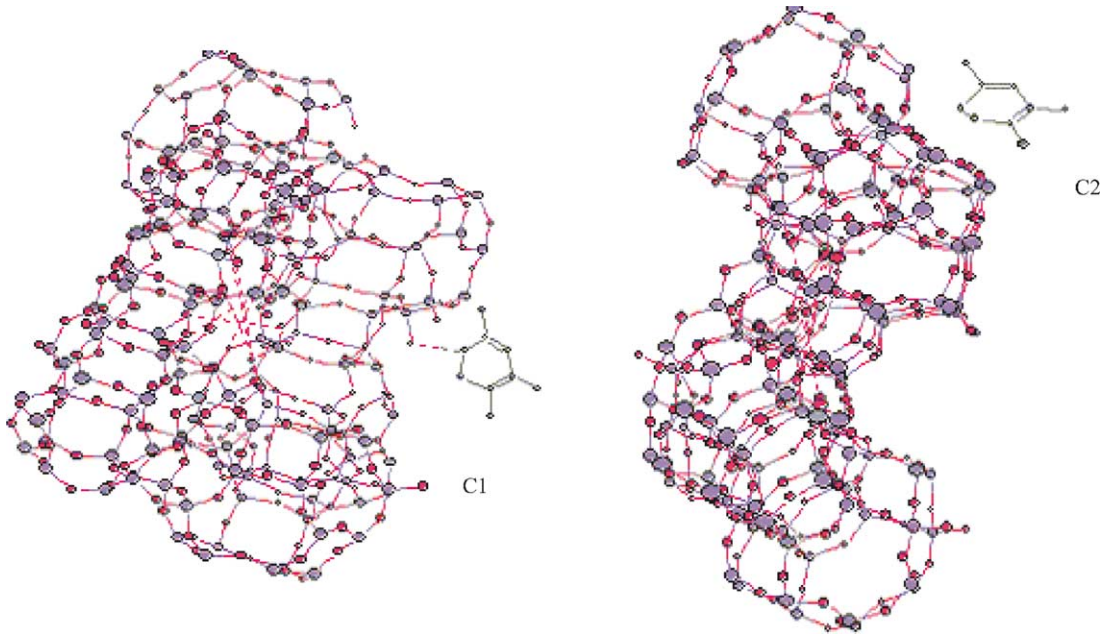

Fig. 14. Positions of carbocations formation outside the supercage (see schemes in Fig. 13).

Table 3
Carbocation formation outside the supercage

	Model					
	C1	C2	C3	C1–Al	C2–Al	C3–Al
Al–OH (Si) bond length (Å)	2.50	2.34	1.91	3.33	3.46	3.04
Steric energy (kcal/mol)	1116.2	1130.4	1133.2	1073.5	1074.9	1078.0

C1, C2 and C3 are the location of the carbocation with fixed structure; C1–Al, C2–Al and C3–Al are the structures considering that the whole structure is relaxed upon carbocation formation.

Regarding the importance of covalent bonding, for large C–O bonds, the position C1 was considered as a representative situation. In this case the C–O distance is close to 2.5 Å, with a 3.07 Å Al–O distance in the structure. If the steric energy is re-evaluated for this case a 1109 kcal/mol is obtained versus the 1116.2 kcal/mol for a ionic bond as reported in Table 3.

Moreover, if a covalent bond is evaluated at the window of a fixed structure, the steric energies are consistently higher from 5.4 to 65 kcal/mol. If this analysis is developed in a relaxed structure with a large C–O covalent bond (3 Å) on a USY, a decrease in the steric energy of near 18 kcal/mol was obtained.

5.1.2. Modeling of the Reduced Window: carbocation/alkoxide formation at the window

For the *Reduced Window* model, the standard enthalpy and the steric energy were calculated, both for fixed and mobile atoms, and this when the 1,2,4-TMB molecules enter the supercage.

In this respect, a calculation of the carbocation formation was developed and this calculation involved the transfer of an acidic proton to the side of the 2H (from TMB) with formation of an alkoxide bond C(TMB)–O(*Reduced Window*) with 1.415 Å short bond and 3 Å long bond, respectively. The later case considers that the Brönsted site was destroyed, as a result of the enlargement of the Al–O bond length in the Al–O–Si structure with this requiring allowance for complete window mobility.

Table 4 reports C–O (Si) and Al–O bond length, steric energies and enthalpy changes. Ads1, Ads2 and Ads3 keys listed in Fig. 15 refer to different possible window location for the incoming TMB molecule. Carbo key refers to the species with a negative charge in O and a positive charge on C atom (C–O bond = 3 Å). Alkox1 represents a configuration resulting of an energy minimization calculation neglecting O or C atoms charges, while Alkox2 a configuration with a 3 Å bond length and Alkox3 a form with a non-set C–O bond length.

Table 4 reports steric energies for the various described species. If one compares Ads1, Ads2 and Ads3 adsorption of 1,2,4-TMB, it can be concluded that Ads3 species is most favored sterically and enthalpically. These results are consistent with the fact that Ads3 is located outside the window and as a result there is no accessibility problem to form Ads3 while Ads1 is located well inside the window thus, experiencing the maximum constrains in terms of accessibility effects.

It can also be noticed that steric energies are much larger for the rigid structure than for the mobile configurations, −44.8 and 129.8 kcal/mol for Alkox2 and Alkox3, respectively. Regarding Alkox1, it is energetically preferred ($\Delta H_f = -3286.8$ kcal/mol) displaying a 13.1 kcal/mol steric energy intermediate between Aldox2 and Aldox3.

Results of this model are, on the matters that concern adsorption/carbocation/alkoxide reaction, well in agreement with the *Complete Window* model. In this sense, both PM3 and MM2 methods confirm the preferred adsorption for 1,2,4-TMB on the outside surface of the cages.

5.1.3. Modeling of Reduced Window—EHMO

The total energy of adsorbed species, E_{total}, can be calculated as the difference between the electronic energy of the system 1,2,4-TMB and surface placed at a finite distance and when the TMB molecule and the USY surface are far away:

$$E_{total} = E_{Reduced\ Window} + E_{TMB} - E_{Reduced\ Window/TMB}$$

Table 4
1,2,4-TMB adsorption and carbocation/alkoxide formation in *Reduced Window* model

	Model						
	Ads1	Ads2	Ads3	Carbo	Alkox1	Alkox2	Alkox3
Bond length (Å)							
C–O (Si)	–	–	–	3.00	1.42	3.00	2.01
Al–O	1.98	1.98	1.96	3.30	3.41	3.43	6.32
ΔH_f (kcal/mol)	−3306.4	−3320.4	−3341.4	−3062.6	−3286.8	−3151.6	−3164.6
Steric energy (kcal/mol)	111.9	104.3	91.6	294.7	13.1	−44.8	129.8

ΔH_f of the window (PM3) = −3344.7 kcal/mol; ΔH_f of the 1,2,4-TMB (PM3) = +1.13 kcal/mol.

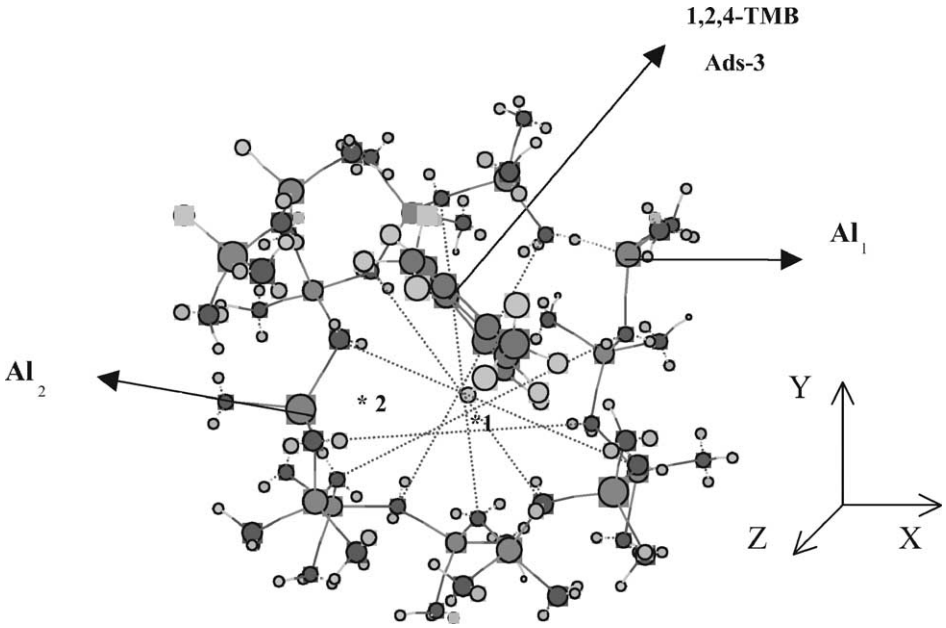

Fig. 15. Adsorption of 1,2,4-TMB in position 3. Ads1 and Ads2 are indicated with '*'.

Coordinates for 1,2,4-TMB (according to the coordinates shown in Fig. 15) are given having C1 placed at the center of the window, following energy minimization using MM2 program. It was found using MM2 that parallel adsorption is not favored with perpendicular interaction being allowed only. This interaction was further analyzed with EHMO (Fig. 16).

Fig. 17A reports the results when 1,2,4-TMB moves forward as described using the *Reduced Window* model. All the changes of energy were evaluated with respect to the initial perpendicular position ($E_{Reduced\,Window} + E_{TMB} = -7170$ eV). The reported figure shows that the forward movement of the TMB molecule in the supercage is a process strongly hindered in the 7.4 Å window. In this respect, an energetic minimum was found in $z = -1.3$ Å (in details in Fig. 17B) and therefore, in that position the formation of carbocation was considered.

Thus, as reported in Fig. 15, the various stages of the carbocation formation and the forward movement of the carbocation in the supercage as viewed with the *Reduced Window* model can be described as follows:

1. TMB moves as a molecule close to an OH superficial group until reaching the$z = 1.3$, $x = -0.1$, $y = -0.4$ coordinates with a change in E_{total} of -3.01 eV.
2. At this position, as described in (1), the H related to Al_1–O–Si group at the window (Fig. 15) approached the

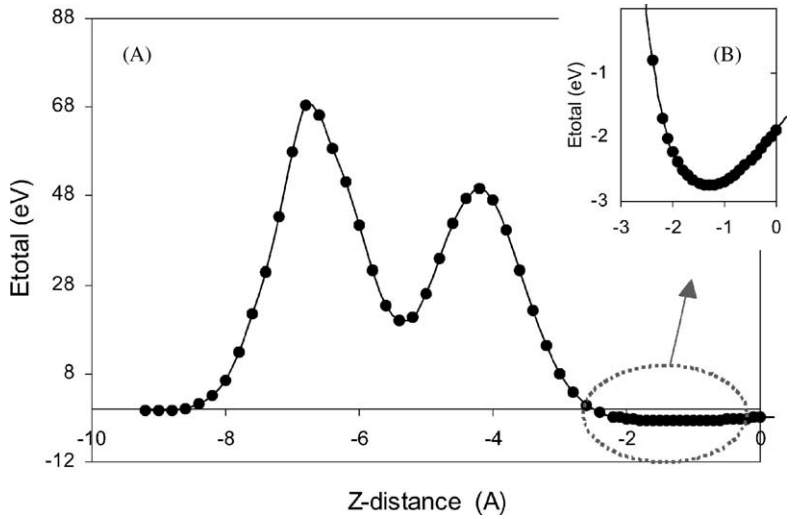

Fig. 16. (A) Energy variation for 1,2,4-TMB movement forward supercage in *Reduced Window* model (calculated by EHMO). (B) Expanded view of (A) section.

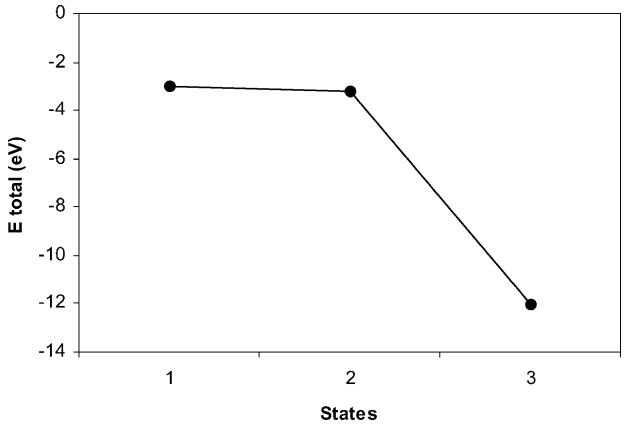

Fig. 17. Carbocation formation for 1,2,4-TMB through *Reduced Window* model (calculated by EHMO). Coordinate: $x = -0.1$, $y = -0.4$, $z = -1.3$. States 1, 2 and 3 as detailed in Section 5.1.3.

C1 in the TMB molecule. This carbon atom changes its configuration (to sp4) with an energy variation for this transition state is −3.22 eV.

3. Completed this, a carbocation is formed with an energy variation of −12.03 eV and this is an indication of strongly favored process.
4. The formed carbocation evolves in the window until $z = -2$ Å and then it moves to $x = -0.7$ Å and $y = -0.4$ Å. Following this, it moves even further until $z = -3$ Å with an energy of −5.35 eV (referred to the initial perpendicular position).
5. Moreover, the carbocation rotates 90° to be able to move further in the zeolite window, with a change of energy of −2.33 eV.
6. Subsequently, it rotates further to move itself in, adopting a perpendicular orientation. At $z = -8$ Å, the calculated change in energy is −8.2 eV.

In summary, the steps that involve the entry of carbocation in the supercage are strongly hindered (endothermic) with the formation of the carbocation being "per se" highly exothermic and all this contribute to the compensation of energies required for the introduction of the carbocation in zeolite window.

5.2. Modeling of cages

Modeling of the cages involves consideration of two possible situations. The first case refers to calculations for a cage still forming an integral part of the original unit cell. This leads to 1,2,4-TMB and cage perpendicular interactions only. The second case considers the cage now removed from the original unit cell with this being viewed as the result of the structure dislocation as promoted by steaming. In this second situation both parallel and perpendicular interactions between 1,2,4-TMB and the cages are allowed. Both MM2 and PM3 method were applied to describe the first case (only perpendicular interactions) while EHMO was employed for describing the second situation (perpendicular and parallel interactions) (Fig. 18).

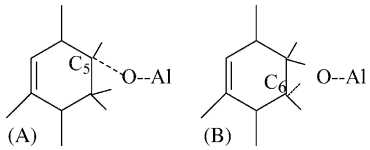

Fig. 18. Covalent bonds studied: (A) covalent-1, (B) covalent-3.

5.2.1. Modeling of Cage 1: MM2 and PM3

TMB adsorption on the *Cage 1* is developed with the assumption that *Cage 1* is an integral part of the crystalline structure (refer to both Figs. 3 and 19) and the 1,2,4-TMB interacts with the zeolite cage adopting a perpendicular orientation only.

Considering the initial steric energy of *Cage 1* model as 51.9 kcal/mol, adsorption of 1,2,4-TMB generates a change of only −4.5 kcal/mol in steric energy on the side of Al–OH–Si.

Table 5 refers to covalent bonds 1, 2, 21 and 3. The numerical keys describe the different carbon atoms in the aromatic ring bonded to the Al–O site. The following is the convention and inter-atomic distances: (a) covalent-1: C5–O–Al, C–O = 1.46 Å, Al–O = 2.14 Å; (b) covalent-2: C5–O–Al, C–O = 1.42 Å, Al–O = 4.23 Å; (c) covalent-21: C6–O–Al, C–O = 2.5 Å, Al–O = 3.91 Å and (d) covalent-3: C6–O–Al, C–O = 1.42 Å, Al–O = 3.86 Å.

Table 5 also reports the steric energies and the enthalpy changes for the various 1,2,4-TMB possible interactions on *Cage 1*, with Covalent structures 2 and 3 being favored, with −13.5 and −10 kcal/mol "SE + $\Delta(\Delta H_f)$" values.

5.2.2. Modeling of Cage 1: EHMO

Modeling of adsorption of the 1,2,4-TMB on *Cage 1* can be completed using EHMO and considering two molecular orientations: aromatic ring perpendicular and parallel (refer to Fig. 19). The parallel orientation is allowed, given in this situation, a partially destroyed USY is considered.

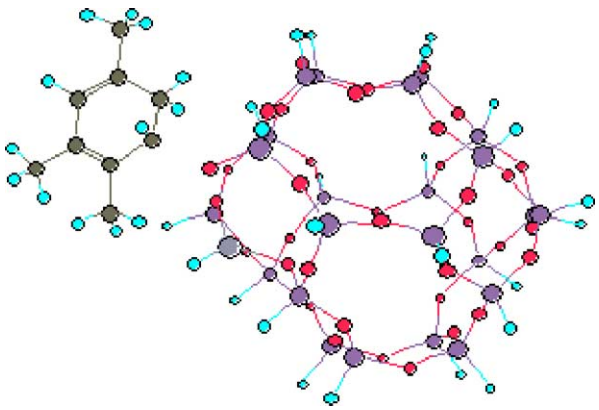

Fig. 19. Carbocation formation in *Cage 1* model.

Table 5
Steric energies and enthalpy changes for adsorption of 1,2,4-TMB on *Cage 1* model (Figs. 18 and 19)

	Al–O (Å)	C–O (Å)	SE[a] (kcal/mol)	ΔSE (kcal/mol)	ΔH_f (kcal/mol)	$\Delta(\Delta H_f)$ (kcal/mol)	Sum[b] (kcal/mol)
Carbocation	3.65	2.03	−45.8	−97.7	−3586.5	128.0	30.3
Covalent-1	2.14	1.46	64.78	12.9	−3671.6	42.9	55.8
Covalent-2	4.23	1.42	−0.87	−52.8	−3675.3	39.3	−13.5[c]
Covalent-21	3.91	2.50	−4.92	−56.9	−3564.9	149.6	92.7
Covalent-3	3.86	1.42	−3.96	−55.9	−3668.6	45.9	−10[c]

The values of enthalpy must be compared with −3713.41 ± 1.13 kcal/mol.
[a] Steric energy.
[b] Sum = ΔSE + $\Delta(\Delta H_f)$.
[c] Preferred forms.

Table 6
Adsorption energies and C–H distances for adsorption of carbocation on *Cage 1*

1,2,4-TMB orientation	Energy (eV)	Distance C5–H (Å)
Perpendicular (2H side)	−0.65	2.43
Parallel	−1.06	2.62

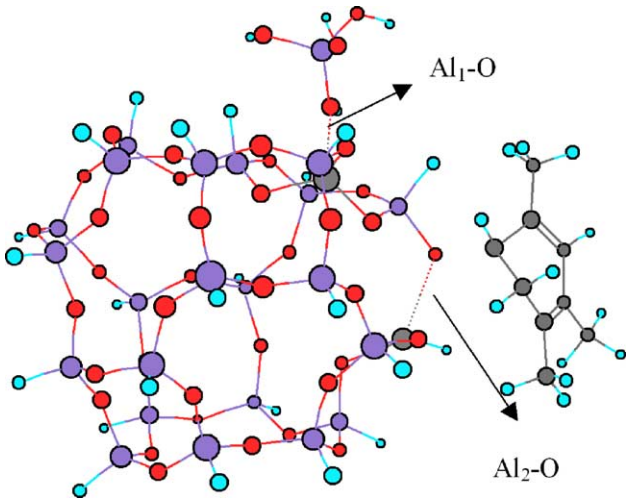

Fig. 20. Carbocation formed with short Al–O bonds in *Cage 2* model (see Table 8).

Table 6 reports the calculated adsorption energies and C–H distances. The adsorption energies were −1.6 and −0.65 eV for parallel and perpendicular, respectively.

These adsorption energies were lower than the ones found when 1,2,4-TMB adsorbed in the window model (−3.01 eV as reported in Section 5.1.3).

5.2.3. Modeling of Cage 2: MM2 and PM3

Cage 2 displays a steric energy of 117.9 kcal/mol and can involve two different bonds: Al_1–O and Al_2–O (Fig. 20). Given the reactive bond is Al_2–O, the perpendicular carbocations can be by the 1H side or by the 2H side of the 1,2,4-TMB molecule.

Tables 7and 8 report steric energies and enthalpy changes for adsorption in *Cage 2* (side of the Al-perpendicular orientation). Two possible Al_1–O bond lengths can be assigned (in the zeolite structure) 2.50 and 4.23 Å. In the first case, the length bond is set in accordance with [28], whereas in the second case the bond is allowed to be relaxed until the minimum energy configuration is reached. This increase of the bond length creates a condition not very favorable for the regeneration of the Brönsted acidic site.

From the reported data it can be observed that the carbocation formation is strongly favored when the structure is modified (−128.3 and −107 kcal/mol, reported in Table 7). When the structure is kept with the Al_1–O bond set at 2.5 Å and the Al_2–O bond is set at 2.5 Å, the change in total energy as a result of carbocation formation is also negative, but lower than in the first case.

Covalent-1 and covalent-2 refer to covalent bond via C5, with a different Al_2–O length bonds (Fig. 18). From the cases reported in Table 7, covalent-1 with a total energy of –81.8 kcal/mol and an Al_2–O bond of 4.22 , is the one displaying the more favorable steric energy.

5.2.4. Modeling of Cage 2—EHMO

Again, and with the aim of representing the 1,2,4-TMB adsorption on a structure partially destroyed, both parallel and perpendicular orientations of the 1,2,4-TMB molecule was allowed.

Table 7
Steric energies and enthalpy changes for adsorption on *Cage 2*: side of the Al-perpendicular

	Al_2–O (Å)	C–O (Å)	SE (kcal/mol)	ΔSE (kcal/mol)	ΔH_f (kcal/mol)	$\Delta(\Delta H_f)$ (kcal/mol)	Sum[a] (kcal/mol)
Carbocation (side of 2H)	4.46	2.04	−115.2	−233.1	−3852.9	104.8	−128.3[b]
Carbocation (side of 1H)	4.28	2.08	−105.3	−223.2	−3841.5	116.2	−107[b]
Covalent-1	4.22	1.42	−7.0	−124.9	−3914.7	43.1	−81.8
Covalent-2	2.07	1.42	139.4	21.5	−3913.4	44.3	65.8

The values of enthalpy must be compared with −3956.6 ± 1.13 kcal/mol. Al_1–O bond set at 4.23 Å.
[a] Sum = ΔSE + $\Delta(\Delta H_f)$.
[b] Preferred forms.

Table 8
Steric energies and enthalpy changes for adsorption of 1,2,4-TMB on *Cage 2* model: side of the Al-perpendicular

	Al_2–O (Å)	C–O (Å)	SE (kcal/mol)	ΔSE (kcal/mol)	ΔH_f (kcal/mol)	$\Delta(\Delta H_f)$ (kcal/mol)	Sum[a] (kcal/mol)
Carbocation side of 1H	4.10	2.06	−63.6	−181.4	−3841.4	116.3	−65.1
Carbocation side of 2H	4.40	2.06	−68.0	−185.9	−3850.4	107.3	−78.6
	2.50	2.19	−38.9	−156.8	−3815.2	142.5	−14.3
	2.40	2.17	−32.7	−150.6	−3813.0	144.7	−5.9
	2.30	2.19	−65.9	−183.8	−3830.8	126.9	−56.8
	2.20	2.19	−55.7	−173.5	−3833.5	124.2	−49.3
Covalent (Al_1–O = 2.05)	2.50	3.00	74.5	−43.4	−3792.2	165.5	122.1
	2.50	2.11	−18.4	−136.3	−3834.4	123.3	−13.0

Al_1–O bond set at 2.50 Å.
[a] Sum = ΔSE + Δ(ΔH_f).

Table 9
Adsorption energies and C–H distances for *Cage 2* model

1,2,4-TMB orientation	Energy (eV)	Distance C5–H (Å)
Perpendicular (2H side)	−0.47	3.20
Parallel	−0.67	3.47

Table 9 reports the adsorption energies and C–H distances for1,2,4-TMB adsorption on *Cage 2*. Adsorption energies for parallel and perpendicular orientation are −0.67 and −0.47 eV, respectively, showing that the TMB adsorption on a structure partially destroyed is energetically favored in both cases as in *Cage 1* model.

5.2.5. Modeling of Cage 3—MM2 and PM3

Table 10 reports steric energies and enthalpy changes for adsorption of 1,2,4-TMB on *Cage 3* model. While the initial steric energy of the *Cage 3* is 52.8 kcal/mol, there are changes in the steric energies and enthalpy changes for adsorption of 1,2,4-TMB. Covalent-1 and covalent-2 formed via C5, and involving different Al–O length bonds (Fig. 18).

In *Cage 10*, although the carbocation formation is allowed (−15.1 kcal/mol) and covalent bonding TMB–cage can develop (−1.3 kcal/mol), the change in energy demonstrates a weakly favored carbocation formation path. Even more interaction of 1,2,4-TMB by its 2H side is clearly preferred (−15.1 kcal/mol versus 205.61 kcal/mol).

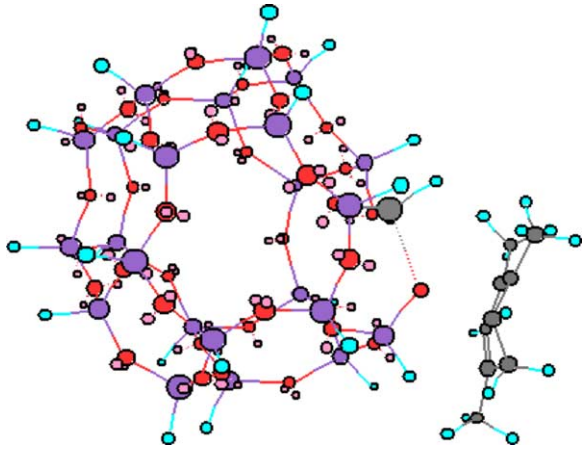

Fig. 21. Carbocation formation in *Cage 3* model.

5.2.6. Modeling of Cage 3—EHMO

Application of the EHMO model led to adsorption energies for 1,2,4-TMB on *Cage 3* model (as shown in Fig. 21) that were all positive. As a consequence of this, *Cage 3* model it was judged was that hypothesized adsorption species were not energetically allowed.

5.2.7. Modeling of Cage 4—MM2 and PM3

Cage 4 was evaluated using MM2 and PM3. Table 11 reports steric energies and enthalpy changes for adsorption of 1,2,4-TMB on this model While the initial steric energy

Table 10
Steric energies and enthalpy changes for adsorption of 1,2,4-TMB on *Cage 3* model

	Al–O (Å)	C–O (Å)	SE (kcal/mol)	ΔSE (kcal/mol)	ΔH_f (kcal/mol)	$\Delta(\Delta H_f)$ (kcal/mol)	Sum[a] (kcal/mol)
Carbocation (side of 2H)	4.00	2.06	−97.3	−150.1	−3581.9	144.6	−5.5[b]
	2.50	2.14	−82.7	−135.4	−3606.2	120.3	−15.1[b]
Carbocation (side of 1H)	3.85	2.16	117.9	65.1	−3586.0	140.5	205.6
Covalent-1	4.01	1.42	−3.9	−56.7	−3669.6	56.9	0.2
Covalent-2	5.82	1.42	−3.6	−46.4	−3681.5	45.1	−1.3[b]

Side of the Al-perpendicular. The values of enthalpy must be compared with −3725.4 ± 1.13 kcal/mol.
[a] Sum = ΔSE + Δ(ΔH_f).
[b] Preferred forms.

Table 11
Steric energies and enthalpy changes for adsorption of 1,2,4-TMB on *Cage 4* model

	Al–O (Å)	C–O (Å)	SE (kcal/mol)	ΔSE (kcal/mol)	ΔH_f (kcal/mol)	$\Delta(\Delta H_f)$ (kcal/mol)	Sum[a] (kcal/mol)
Carbocation (side of 2H)	3.66	2.16	184.3	66.9	−3492.6	136.9	203.8
Carbocation (side of 1H)	2.00	2.35	226.8	109.4	–	–	–
Covalent-1	3.34	1.42	64.6	−52.8	−3570.4	59.1	6.3[b]
Covalent-2	2.75	1.44	103.0	−14.4	−3568.0	61.4	47.0

Side of the Al-perpendicular. The values of enthalpy must be compared with -3628.35 ± 1.13 kcal/mol.
[a] Sum $= \Delta SE + \Delta(\Delta H_f)$.
[b] Preferred forms.

of *Cage 4* is 117.4 kcal/mol, all adsorption energies were positive. For instance, TMB covalent bonding is in the least hindered conditions display a total energy of 6.3 kcal/mol. It was argued on this basis that no interaction takes place at the site, at the selected conditions.

6. Discussions

Steaming is a frequent technique used in the manufacture of USY zeolites. Steaming to stabilize the zeolite generates mesopores and fractures in the zeolite structure. It is thus, expected that steaming leads to a much larger accessible zeolite area.

Researchers argued that zeolite steaming can be linked to unusually strong Brönsted acid sites, or/and increased influence of Lewis acid centers playing a role in initiation reactions [29].

However, the more recent evidence points to steaming affecting the sorption properties of entire sodalite units, which can be destroyed during hydrothermal dealumination [30]. Fernández et al. [31] indicated that before steaming, the zeolite has micropores of uniform sizes and during the process of dealumination, super-micropores (7–20 Å) and/or mesopores can be produced depending on selected conditions. Cavalcante et al. [32] observed no significant difference in diffusivities between C6 to C10 in USY sample. These authors argued that this might be due to the larger pore opening of the mesoporous structure created by the dealumination of the zeolite Y framework.

Thus, increased activity in H-USY is more likely the result of enhanced cracking reaction in zeolite due to structural changes in zeolites and reduced pore-diffusion limitation [33]. Beyerlein et al. [1,34] studied the effect of steaming on the defect structure and acid catalysis of protonated zeolites. Steam treatments induced to an inhomogeneous distribution of mesopores, which occurred concomitantly with further zeolite dealumination. Such inhomogeneities were observed among different USY grains as well as within single grains. In regions with high defect concentration, mesopores "coalesced" to form channels and cracks which, upon extended hydrothermal treatment, ultimately defined the boundaries of fractured crystallite fragments. The predominant fate of aluminum ejected from lattice sites appeared to be closely associated with dark bands, which often decorate these newly formed fracture boundaries. But as Janssen et al. [35] reported, fracture of Y crystals is seen only when a very severe steaming is applied.

On the same line of thought, Kuhene et al. [36] noted that only active sites near the zeolite surface contribute to the activity. The formation of mesopores and fractures could increase the observed catalytic activity by increasing the external surface area for molecules to diffuse into the zeolite micropores. In other words, a greater number of the active sites (within the micropores) are close to the external surface and can participate in the reaction. These authors highlight that diffusion limitation within the micropores, or the apparent activation energies between Y and USY zeolite form may not need be different. Steaming or chemical dealumination makes a greater number of active sites close to regions accessible by diffusion.

Accordingly during steaming mesopores, crevices and fissures are formed augmenting the accessible zeolite surface area. This creates mesopores reduces diffusion, and consequently, increases activity.

In the process of catalytic cracking, the ratio of catalyst to oil is sufficiently low (between 3 and 8) to saturate all catalyst surfaces, if adsorption strength allows [37].Table 12 reports adsorption constants at 450 °C measured experimentally in our laboratory for 1,2,4-TMB, 1,3,5-TMB, toluene,

Table 12
Parameters obtained for different molecules adsorption on USY [38]

Molecule/surface	Critical diameter (Å)	Adsorption constant (m^3/kg USY) at 450 °C	Total covered area per adsorbed molecules (m^2/g USY)
Benzene/USY	5.5	0.0196	71.2
Toluene/USY	6.7	0.0228	122.8
p-Xylene/USY	6.7	0.0256	138.2
1,2,4-TMB/USY	7.4	0.0286	116.9
1,3,5-TMB/USY	8.6	0.0289	313.1

benzene and xylene adsorption on HY catalysts respectively. A more detailed description of the method used in the determination of adsorption constants can be found in [38]. Temperature and pressure were selected to mimic reaction conditions. A "total covered area" was calculated just taking into consideration the molecular critical diameter without concern for molecular shape or the number and nature of interacting parts of the molecule and actives sites in the zeolite. This was performed in order to have an idea of $surface_{covered}/surface_{free}$ ratio for zeolites. Specific surface areas for the FCC catalysts studied were 545 m^2/g USY (or 169 m^2/g of catalyst).

According to Table 12, it seemed that a small fraction of the total area is used in adsorption process under reaction conditions. This latter agree with a publication of Weisz [39], who indicated that is important to differentiate between the large bulk of total immobilization sites ("jump sites") and the usually much smaller number of catalytic sites used under reaction conditions. Then, when values presented in Table 12 are related to theoretical results reported in this work, is simpler realize that the carbocation is formed easier in the window.

In agreement with this, recent work from Auerbach [40] emphasizes that benzene diffusion in zeolites with cation and window sites is dominated by window-to-window jumps more than cage-to-cage jumps. Furthermore, recent simulations on lattice models [41] have provided qualitative insights regarding the relationship between fundamental site-to-site jumps and the resulting loading dependences of diffusion. While most studies model diffusion in zeolites, a new emphasis on modeling orientation dynamics has emerged, to reveal more subtle aspects of zeolite structures including possible Al distributions. The main aim of this work is to present an approach to deal with this problem.

Results of the present study shows that 1,2,4-TMB adsorption and carbocation/alkoxide formation using a *Reduced Window* model (Table 4, Fig. 17), and PM3, MM2 and EHMO methods confirm a preferred adsorption on the outside surface of the cages. Also, it is shown that 1,2,4-TMB adsorption on partially destructed zeolite is energetically favorable.

Furthermore MM2 and PM3 calculations, in agreement with EHMO results, points towards a preferred covalent bonding in *Cage 1* model, carbocation stabilization in *Cage 2* with and without structure distortion, carbocation preferred interaction in *Cage 3*, and no stable interacting form in *Cage 4*. Thus, the 1,2,4-TMB has to have inside of the supercage a considerable high energy barrier to surpass and most likely reacts outside and/or at the window of the supercage, with carbocation formation and structures with C–O bonds with a certain mixed covalent/ionic character.

It is important to note that *Cages 3* and *4* form the window walls. These calculations imply that the carbocation is preferentially formed on the left side of the window, where the Al of *Cage 3* is located, whereas covalent bonding is preferred in the right side of the window. However, the 1,2,4-TMB reaction is not favored, because energies are positive. When the *Cage 3* results are analyzed, the sum is negative (−15 kcal/mol), at the distances C–O there presented (2.14 Å). This fact implies that the molecule does not access the supercage and reacts at the window only. The location of the carbocation in *Cage 3* model demonstrates that, when a crystalline ideal structure is considered, this carbocation is not formed by steric hindrance of the other cages of the window. All the values of enthalpy changes are positive, whereas of the steric energies vary: positive and negative values.

Regarding the result of this study, a high barrier to introduce 1,2,4-TMB inside the supercage was found, and this when the window is not relaxed and its diameter is 7.4 Å. However, no diffusional problems were found for 1,2,4-TMB and diffusional constraints were reported for both isomerization/disproportionation of 1,3,5-TIPB using a USY catalyst [42,43]. Furthermore, it was observed that selectivities do not follow thermodynamics especially for disproportionation reactions [44]. This fact implies that the model of an unrelaxed window does not explain completely the experimental results and another basis, like the one presented in this study, to explain the data is needed to specifically account for disproportionation reactions, and reported earlier [45].

In summary, calculation results presented in this work support the idea of a high probability of carbocation formation and overall reaction in fragments removed from the zeolite structure. This relaxation is enough to allow structure mobility and TMB accessibility to the acidic sites.

7. Conclusions

This work reports the interaction between 1,2,4-TMB and USY. The zeolite is modeled using the complete exposed USY structure of one unit cell constituted by eight sodalite cages, 16 hexagonal prisms bridging the sodalite cages and the formed supercage. The experimental Si/Al ratio was used in the calculations using MM2, PM3 and extended Hückel methods.

The following are the most relevant conclusions of the present study:

1. Calculations developed show that 1,2,4-TMB adsorption takes place at the 7.4 Å windows of steamed HY, especially on the acidic sites involving Al–OH–Si bonds.
2. 1,2,4-TMB adsorption on the outside surface of the cages is energetically favored.
3. Carbocations can also be formed on the window or the external structure. This can lead to isomerization mainly taking place in the external surface of the zeolite structure.
4. 1,2,4-TMB transport into a 7.4 Å window of a Y zeolite is severely hindered and restricted. Thus, it appears steaming relaxes the USY structure to allow this 1,2,4-TMB evolution.

Acknowledgements

We are very grateful to the financial support provided by Universidad Nacional del Sur, the Consejo Nacional de Investigaciones Científicas y Técnicas (CONICET), and the Natural Sciences and Research Council of Canada (NSREC).

References

[1] R. Beyerlein, C. Choi-Feng, J. Hall, B. Huggins, G. Ray, Top. Catal. 4 (1997) 27.
[2] S. van Donk, A. Janssen, J. Bitter, K. de Jong, Catal. Rev. 45 (2003) 297.
[3] J. Scherzer, in: T.E. White, R.A. Della Betta, E.G. Derouane, R.T.K. Baker (Eds.), Catalytic Materials: Relationship Between Structure and Activity, ACS Symp. Ser. 248, American Chemical Society, Washington, DC, 1984, p. 157.
[4] A. Gola, B. Rebours, E. Milazzo, J. Lynch, F. Benazzi, S. Lacombe, L. Delevoye, C. Fernández, Microp. Mesop. Mater. 40 (2000) 73.
[5] H. Hong, D. Coster, F. Chen, J. Davis, J. Fripiat, in: L. Buczi (Ed.), New Frontiers in Catalysis, Proceedings of the 10th Congress on Catalysis, Budapest, 19–24 July 1992, Elsevier Amsterdam, 1993, pp. 1159–1170.
[6] P. Jacobs, Carboniogenic Activity of Zeolites, Elsevier, Amsterdam, 1977.
[7] R. Carvajal, P.-J. Chu, J.H. Lunsford, J. Catal. 125 (1990) 123.
[8] A. Biaglow, D. Parillo, G. Kokotailo, R. Gorte, J. Catal. 148 (1994) 213.
[9] H. Kung, B. Williams, S. Babitz, J. Miller, W. Haag, R. Snurr, Top. Catal. 10 (2000) 59.
[10] H. Kung, B. Williams, S. Babitz, J. Miller, R. Snurr, Catal. Today 52 (1999) 91.
[11] B. Williams, S. Babitz, J. Miller, R. Snurr, H. Kung, Appl. Catal. A 177 (1999) 161.
[12] H. Stach, U. Lohse, H. Thamm, W. Schirmer, Zeolites 6 (1986) 74.
[13] J. Scherzer, Octane-Enhancing Zeolite FCC Catalysts: Scientific and Technical Aspects, Dekker, New York, 1990.
[14] V. Kazansky, M. Frash, R. van Santen, Catal. Lett. 28 (1994) 211.
[15] A. Corma, J. Planelles, J. Sanchez-Martin, F. Tomas, J. Catal. 93 (1985) 30.
[16] C. Choi-Feng, J. Hall, B. Huggins, R. Beyerlein, J. Catal. 140 (1993) 395.
[17] Grace Davison Guide to Fluid Catalytic Cracking, Part 2 (http://www.sts-aiche.org/pepo0402.pdf).
[18] V. Kazansky, L. Senchenya, J. Catal. 119 (1989) 108.
[19] R. Hoffmann, Solids and Surfaces: A Chemist's View of Bonding in Extended Structures, CUCH, New York, 1988 and references therein.
[20] A. Anderson, R. Hoffmann, J. Chem. Phys. 60 (1974) 4271.
[21] J. Kamber, L. Forrs, G. Calzaferri, J. Phys. Chem. 93 (1989) 5366.
[22] A.B. Anderson, J. Chem. Phys. 62 (1975) 1187.
[23] A.B. Anderson, J. Mol. Catal. 54 (1989) 281.
[24] W. Lotz, J. Opt. Soc. Am. 60 (1970) 206.
[25] A. Vela, L. Gázquez, J. Phys. Chem. 92 (1985) 5688.
[26] R. Hoffmann, J. Am. Chem. Soc. 107 (1985) 4440.
[27] P. Bagus, H. Schaefer, C. Bauschlinder Jr., J. Chem. Phys. 78 (1983) 1390.
[28] D. Lide (Ed.), Handbook of Chemistry and Physics, 76th ed., 1995–1996.
[29] A. Corma, J. Planelles, J. Sanchez-Marin, F. Tomas, J. Catal. 93 (1985) 30.
[30] H. Stach, U. Lohse, H. Thamm, W. Schirmer, Zeolites 6 (1986) 74.
[31] C. Fernández, J. Vedrine, J. Grosmangin, G. Szabo, Zeolites 6 (1986) 484.
[32] C. Cavalcante, N. Silva, E. Souza-Aguiar, E. Sobrinho, Adsorption 9 (2003) 205.
[33] P. Hopkins, J. Miller, B. Meyers, G. Ray, R. Roginski, M. Kuehne, H. Kung, Appl. Catal. A 136 (1996) 29.
[34] C. Choi-Feng, J. Hall, B. Huggins, R. Beyerlein, J. Catal. 140 (1993) 395.
[35] A. Janssen, A. Koster, K. de Jong, Angew. Chem. Int. Ed. 40 (6) (2001) 1102.
[36] M. Kuehne, S. Babitz, H. Kung, J. Miller, Appl. Catal. A 166 (1998) 293.
[37] F. Hershkowitz, P. Madiara, Ind. Eng. Chem. Res. 32 (1993) 2969.
[38] J. Atias, G. Tonetto, H. De Lasa, Int. J. Chem. React. Eng. 1 (2003) A50.
[39] P. Weisz, Eng. Chem. Res. 34 (1995) 2692.
[40] S. Auerbach, F. Jousse, D. Vercauteren, in: C. Catlow, R. Van Santen, B. Smith (Eds.), Computer Modelling of Microporous Materials.
[41] R. Millini, Catal. Today 41 (1998) 41.
[42] S. Al-Khattaf, H. de Lasa, Appl. Catal. A (2002) 139.
[43] J. Atias, G. Tonetto, H. de Lasa, Ind. Eng. Chem. Res. 42 (2003) 4162.
[44] E. Kikuchi, T. Matsuda, H. Fujiki, Y. Morita, Appl. Catal. 11 (1984) 331.
[45] G. Tonetto, J. Atias, M.L. Ferreira, H. de Lasa, Appl. Catal. A, October 2003, in press.